Mimetic finite difference methods for diffusion equations on non-orthogonal AMR meshes*

Konstantin Lipnikov† Jim Morel* Mikhail Shashkov*

March 28, 2003

Abstract

Mimetic discretizations based on the support-operators methodology are derived for non-orthogonal quadrilateral adaptive meshes. The second-order convergence rate on non-smooth meshes is verified with numerical examples.

1 Introduction

The support operators (SO) method has been used to generate both 2-D and 3-D cell-centered diffusion discretizations on non-orthogonal meshes [15, 8, 11, 10]. The SO method can be applied to many forms of the diffusion equation, but it suffices to consider the following first-order form of the diffusion equation:

$$\mathrm{div}\ \mathbf{F} = Q\,, \tag{1.1a}$$

$$\mathbf{F} = -\mathbf{D}\ \mathrm{grad}\ \phi, \tag{1.1b}$$

where ϕ denotes a scalar function that we refer to as the intensity, $\mathbf{F}$ denotes a vector function that we refer to as the flux, $\mathbf{D}$ denotes a diffusion tensor, and Q denotes a source function. We use the term "cell centered" to indicate a discretization that is conservative over each cell in the mesh. It does not necessarily imply that there are only cell-center intensity unknowns. For instance, there are actually two versions of the SO method: one that has intensity unknowns located only at cell centers [15], and one that has them located at both cell centers and face centers [11]. These methods are equivalent in the sense that they yield identical cell-center intensity solutions, but the former method has a dense diffusion matrix, while the latter method has a banded diffusion matrix. The latter method is referred to as the local SO method.

The purpose of this paper is to use the local support-operators method to generate diffusion discretizations on non-orthogonal quadrilateral meshes having hanging nodes. A hanging node is illustrated in Fig 1. Hanging-node meshes are generally used in adaptive mesh refinement algorithms [7, 18, 13, 14]. Note that a hanging

*The work was performed at Los Alamos National Laboratory operated by the University of California for the US Department of Energy under contract W-7405-ENG-36. (LA-UR-03-1765)

†Los Alamos National Laboratory, MS B284, Los Alamos, NM, 87545. Email: `lipnikov@t7.lanl.gov`, `jim@lanl.gov`, `misha@t7.lanl.gov`.

node occurs when two cells share a face with one cell. We do not allow any cell to share a face with more than two cells, or equivalently, there is never more than one hanging node associated with an interface. This is a restriction motivated by considerations of both simplicity and accuracy that is usually seen in quadtree-based adaptive-mesh algorithms [18]. While the vast majority of existing AMR schemes use orthogonal meshes, it is clear that non-orthogonal mesh schemes are more versatile. Non-orthogonal hanging-node meshes have been used in adaptive Arbitrary Lagrangian-Eulerian (ALE) hydrodynamics algorithms [1]. Our scheme would be suitable for coupled radiation diffusion/hydrodynamics calculations on such meshes.

Our purpose here is not to develop such an AMR diffusion algorithm *per se*, but rather to develop an SO method suitable for use in such an algorithm. The development of any AMR algorithm requires a posteriori error estimation technique [17, 5]. The development of an SO-compatible posteriori error estimation technique is beyond the scope of this paper. Thus, rather than refine to optimally decrease the error in our convergence studies, we simply start with a multi-level hanging-node mesh and carry out a refinement step by increasing the refinement level in each cell by one. This is later demonstrated in detail.

The local SO method is particularly amenable to hanging-node meshes, because the discretization process occurs in two steps. The first step is to consider each cell in the mesh as an independent domain and generate an independent discretization for each cell. The second step is to obtain a global discretization by imposing continuity of the intensity and continuity of the normal component of the flux across cell interfaces. The first step yields equations for the cell-center intensities and the second step yields equations for the face-center intensities. Since each cell in a hanging-node mesh is a quadrilateral, the first step in applying the SO method is identical to that for standard quadrilateral meshes. However, imposing continuity of the intensity and continuity of the normal component of the flux is not straightforward on hanging-node meshes because the intensity and flux unknowns do not coincide as they do on standard meshes. Thus, the main task before us is to determine how to impose continuity of the intensity and the normal component of the flux at three-cell hanging-node interfaces.

The remainder of this paper is organized as follows. In Sec. 2, we first describe the local support-operators method for quadrilateral meshes in Cartesian geometry, and show how it is generalized for meshes with three-cell hanging-node interfaces. In Sec. 2.1, we next give an analogous description for quadrilateral meshes in R-Z geometry . Our solution technique, which is the same for both Cartesian and R-Z geometries, is described in Sec. 3. Computational results are given in Sec. 4, followed by conclusions and recommendations for future work in Sec. 5.

2 Support-operators method

In this section we describe the support-operators (SO) method. We begin by introducing vector spaces of discrete functions together with inner products. Then, we derive a discrete approximation to the divergence operator which we call the *prime* operator. The approximation to the gradient operator (the *derived* operator) will follow naturally from the Gauss-Green formula.

For the discretization of (1.1), we denote by $\mathcal{T}_h = \{e_1, e_2, \ldots, e_N\}$ a *shape regular*

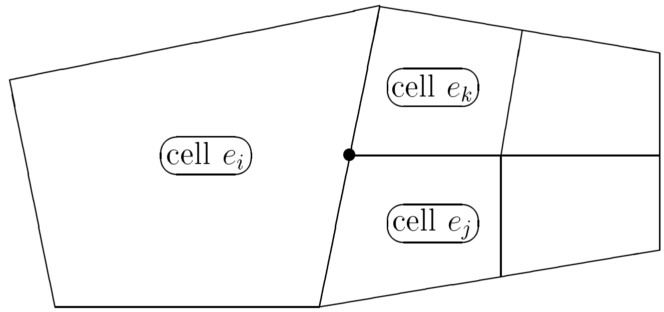

Figure 1: Interface between three cells with a hanging node.

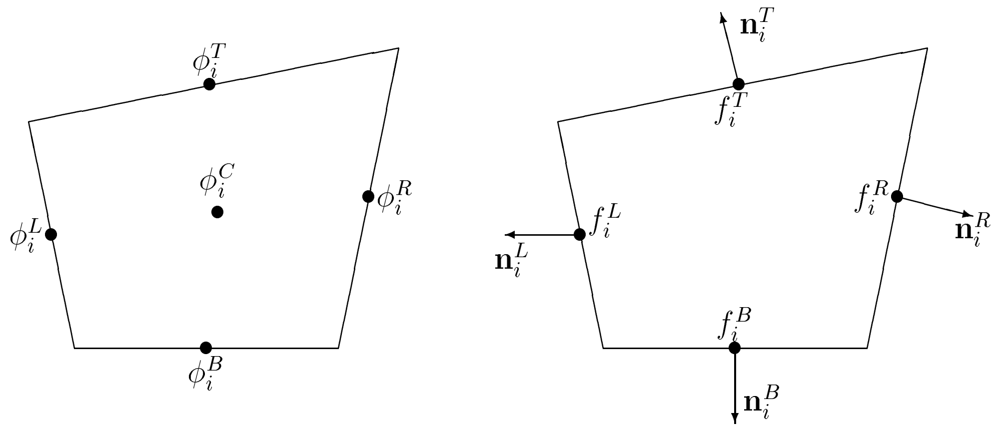

Figure 2: Location of scalar and vector component unknowns.

partition (see [4, p. 113, Remark 2.2]) of $\bar{\Omega}$ into convex quadrilateral cells. Generally speaking, the partition $\mathcal{T}_h$ may be non-conforming. In this case we assume additionally that each mesh edge has at most one hanging node. A few examples of shape regular grids are shown in Section 5.

Our next step is to define the discrete unknowns. Each mesh cell is assumed to be homogeneous, but material properties (diffusion tensor) may vary between cells. As shown in Fig 2, the intensities (scalars) are defined at both cell centers, ϕ_i^C, and the edge centers, ϕ_i^R, ϕ_i^T, ϕ_i^L, ϕ_i^B. The vectors are defined in terms of edge-normal components located at the midpoints of cell edges, f_i^R, f_i^T, f_i^L, f_i^B. For instance, f_i^R denotes the dot product of $\mathbf{F}$ with the outward unit normal $\mathbf{n}_i^R$ located at the center of the right edge of the i-th cell, i.e. $f_i^R = \mathbf{F} \cdot \mathbf{n}_i^R$. The other edge-normal components are defined in a similar way.

Note that the full vector can be recovered at each corner of the i-th mesh cell from two components located on edges that share that corner. We denote the recovered vectors by $\mathbf{F}_i^{RT}$, $\mathbf{F}_i^{LT}$, $\mathbf{F}_i^{LB}$, and $\mathbf{F}_i^{RB}$.

The quantities defined above are uniquely associated with a single cell. The next step is to derive approximations to the divergence and the gradient operators over the i-th cell. We use the Gauss-Green formula

$$\int\limits_{e_i} \mathbf{H} \cdot \mathrm{grad}\psi \, \mathrm{d}V + \int\limits_{e_i} \mathrm{div}\mathbf{H} \, \psi \, \mathrm{d}V = \int\limits_{\partial e_i} \psi \, \mathbf{H} \cdot \mathbf{n} \, \mathrm{d}A \tag{2.1}$$

where ψ is an arbitrary scalar function, $\mathbf{H}$ is an arbitrary vector function, and $\mathbf{n}$ denotes the outward unit normal associated with ∂e_i. We assume that $\psi = 1$ and the vector $\mathbf{H}$ has the same mesh locations as the flux vector $\mathbf{F}$. Then, the central point quadrature rule gives us the formula for a discrete divergence operator DIV over cell e_i:

$$(\mathrm{DIV}\,\mathbf{H})_i = \frac{1}{V_i}\left(h_i^R A_i^R + h_i^T A_i^T + h_i^L A_i^L + h_i^B A_i^B\right) \tag{2.2}$$

where A_i^R denotes the edge length associated with the right edge of the i-th cell and V_i denotes the cell area. Note that the discrete divergence operator is exact when $\mathbf{H}$ is a linear vector function [15].

Now, we derive a discrete gradient operator GRAD which satisfy a discrete version of the Green formula. The first integral in (2.1) is discretized using the values of discrete vector functions recovered at the corners of e_i:

$$\begin{aligned} -\int\limits_{e_i} \mathbf{H}\cdot \mathrm{grad}\psi\,\mathrm{d}V \;&=\; \int_{e_i} \mathbf{H}\cdot \mathbf{D}_i^{-1}\mathbf{G}\,\mathrm{d}V \\ &\approx\; (\mathbf{H}_i^{RT}\cdot \mathbf{D}_i^{-1}\,\mathbf{G}_i^{RT})\,V_i^{RT} + (\mathbf{H}_i^{LT}\cdot \mathbf{D}_i^{-1}\,\mathbf{G}_i^{LT})\,V_i^{LT} \\ &\quad+ (\mathbf{H}_i^{LB}\cdot \mathbf{D}_i^{-1}\,\mathbf{G}_i^{LB})\,V_i^{LB} + (\mathbf{H}_i^{RB}\cdot \mathbf{D}_i^{-1}\,\mathbf{G}_i^{RB})\,V_i^{RB} \end{aligned} \tag{2.3}$$

where $\mathbf{G} = -\mathbf{D}\,\mathrm{grad}\psi$, V_i^{RT} denotes area weight associated with the right-top corner, and $\mathbf{D}_i$ is the value of tensor $\mathbf{D}$ at the mass center of e_i. The sum of area weights equals to the total cell area. Moreover, these weights should provide a sufficiently accurate quadrature rule. In the case of a rectangular cell, each corner weight is defined as one-quarter of the cell area. In the case of an arbitrary quadrilateral cell, the corner weight equals half of the area of the triangle associated with the corner. The triangle is uniquely defined by two cell edges that share the corner.

Simple rules of linear algebra allow us to express the dot product of two vectors via their components. Let $\mathbf{n}_i^R = (n_{ix}^R,\, n_{iy}^R)^t$ be the normal vector associated with the right edge of e_i. Then,

$$\mathbf{H}_i^{RT}\cdot \mathbf{D}_i^{-1}\,\mathbf{G}_i^{RT} = \left[M_i^{RT}\right]^{-t}\begin{bmatrix} h^R \\ h^T \end{bmatrix}\cdot \mathbf{D}_i^{-1}\left[M_i^{RT}\right]^{-1}\begin{bmatrix} g^R \\ g^T \end{bmatrix}, \tag{2.4}$$

where M_i^{RT} is the matrix defined by (see [11] for details):

$$M_i^{RT} = \begin{bmatrix} n_{ix}^R & n_{iy}^R \\ n_{ix}^T & n_{iy}^T \end{bmatrix}.$$

Note that equations (2.3) and (2.4) define the inner product in the space of discrete fluxes. Substituting (2.4) into the right hand side of (2.3), we get

$$\int\limits_{e_i} \mathbf{H}\cdot \mathbf{D}^{-1}\mathbf{G}\,\mathrm{d}V \;\approx\; < M_i\,\vec{h}_i,\ \vec{g}_i > \tag{2.5}$$

where $\vec{h}_i,\, \vec{g}_i \in \Re^4$, $\vec{h}_i = (h_i^R,\, h_i^T,\, h_i^L,\, h_i^B)^t$, are vectors of discrete fluxes associated with the cell e_i, M_i is a 4×4 matrix, and $<\cdot\,,\,\cdot>$ denotes the inner product in $\Re^4$. The matrix M_i is the result of algebraic assembling of symmetric positive definite 2×2 matrices $[M_i^\alpha]^{-t}\,\mathbf{D}_i\,[M_i^\alpha]^{-1}$, $\alpha = RT, LT, LB$ and RB, with corresponding weights V_i^α from (2.3). Note that M_i is the symmetric positive definite matrix and it is diagonal for the rectangular cell.

The second integral in (2.1) is discretized using the definition of the discrete divergence operator:

$$\int\limits_{e_i} \mathrm{div}\mathbf{H}\,\psi\,\mathrm{d}V \approx \left(h_i^R A_i^R + h_i^T A_i^T + h_i^L A_i^L + h_i^B A_i^B\right)\psi_i^C. \tag{2.6}$$

Finally, the boundary integral in (2.1) is discretized with the central point quadrature rule:

$$\int\limits_{\partial e_i} \psi\,\mathbf{H}\cdot\mathbf{n}\,\mathrm{d}A \approx \psi_i^R h_i^R A_i^R + \psi_i^T h_i^T A_i^T + \psi_i^L h_i^L A_i^L + \psi_i^B h_i^B A_i^B. \tag{2.7}$$

The components of the discrete gradient operator GRAD are obtained by substituting the right-hand sides from (2.3), (2.6), and (2.7) into the Green formula (2.1) and requiring that the resulting discretized identity hold for all values of discrete $\mathbf{H}$ and ψ. More specifically, the discrete identity results in

$$(\mathrm{GRAD}\,\psi)_i = M_i^{-1} A_i\,(\vec{\psi}_i - \psi_i^C\,\vec{e}) \tag{2.8}$$

where A_i denotes the diagonal matrix with entries A_i^R, A_i^T, A_i^L and A_i^B, $\vec{e} = (1,1,1,1)^t$, and $\vec{\psi}_i = (\psi_i^R,\ \psi_i^T,\ \psi_i^L,\ \psi_i^B)^t$ is the vector of scalars associated with edges of the cell e_i. In the case when e_i is a rectangle, the matrix M_i is diagonal and formula (2.8) yields a simple expression for each component of the discrete gradient operator. Note that equation (2.8) is exact when ψ is a linear function [15].

Combining formulas (2.2) and (2.8), we obtain a local discretization for the original diffusion equation:

$$\begin{aligned} (\mathrm{DIV}\,\mathbf{F})_i &= Q_i, \\ \vec{f}_i &= (\mathrm{GRAD}\,\phi)_i \end{aligned} \tag{2.9}$$

where $\vec{f}_i = (f_i^R, f_i^T, f_i^L, f_i^B)^t$ and Q_i denotes a value (for instance, integral average) of the source function in the i-th cell. The global discretization can be achieved by imposing continuity conditions for primary variables $\mathbf{F}$ and ϕ across cell interfaces. We require that the discrete version of the integral identity (2.1) holds over the entire mesh. It is not difficult to see that this requirement will be met if the sum over all cells of (2.7) leaves only outer boundary contributions due to cancellation of the interior mesh contributions. For instance, let the cell e_i has a common boundary with cells e_j and e_k as shown on Fig. 3. Then, the boundary terms associated with the common interface will cancel if

$$f_i^R A_i^R \phi_i^R = -f_j^L A_j^L \phi_j^L - f_k^L A_k^L \phi_k^L. \tag{2.10}$$

The negative sign in (2.10) occurs because the edge normals associated with f_i^R and f_j^L (resp., f_i^R and f_k^L) are opposite in direction. If we enforce continuity of fluxes,

$$f_i^R = -f_j^L = -f_k^L, \tag{2.11}$$

we end up with a continuity condition for intensities:

$$A_i^R \phi_i^R = A_j^L \phi_j^L + A_k^L \phi_k^L. \tag{2.12}$$

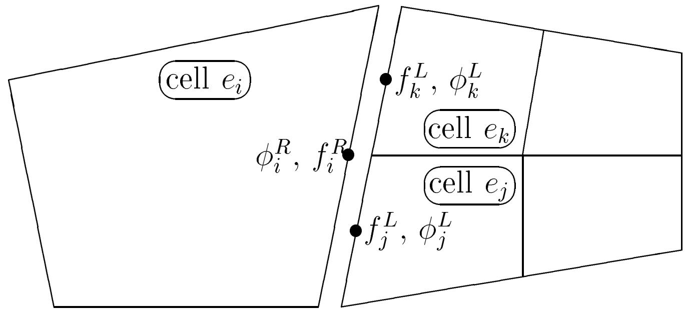

Figure 3: Inner edge with a hanging node.

In the case of only two neighboring cells e_i and e_j with a common edge (for instance, the right edge for e_i), the continuity conditions are

$$f_i^R = -f_j^L \qquad \text{and} \qquad \phi_i^R = \phi_j^L. \tag{2.13}$$

The system of equations (2.9) – (2.13) is closed by imposing the boundary conditions. The Dirichlet boundary conditions specify the intensities associated with the boundary edges. The Neumann boundary conditions prescribe values to the normal components of fluxes. For the sake of simplicity, we assume that the homogeneous Dirichlet boundary condition is given on $\partial\Omega$.

2.1 SO on quadrilateral meshes in $r - z$ geometry

The detailed generalization of the SO method to $r - z$ geometry has been done in [11]. In this section we briefly recall the basic results. The elliptic equation in $r - z$ coordinates reads

$$-\frac{1}{r}\frac{\partial}{\partial r}\left(r\mathbf{D}\frac{\partial\phi}{\partial r}\right) - \frac{\partial}{\partial z}\left(\mathbf{D}\frac{\partial\phi}{\partial z}\right) = Q. \tag{2.14}$$

The basic scheme of the SO method is invariant with respect to a coordinate transformation. However, the expressions for edge lengths and triangle areas depend on the particular coordinate system. In $r - z$ coordinate system, it is useful to introduce vector $\vec{\xi} = (r,\, z)^t$. Then

$$A_i^R = \pi\left(r_i^{RT} + r_i^{RB}\right)\left\|\vec{\xi}_i^{RT} - \vec{\xi}_i^{RB}\right\|$$

where the symbol $\|\cdot\|$ denotes the Euclidean norm in $\Re^2$, and $\vec{\xi}_i^{RT}$ denotes $r - z$ coordinates of the right-top corner of the i-th cell. The other cell lengths are defined by analogy. The area of the triangles with vertices $\vec{\xi}_i^{RT}$, $\vec{\xi}_i^{RB}$ and $\vec{\xi}_i^{LT}$ is given by

$$V_i^{RB} = \frac{\pi}{3}\left|(\vec{\xi}_i^{RB} - \vec{\xi}_i^{RT}) \times (\vec{\xi}_i^{LT} - \vec{\xi}_i^{RT})\right|(r_i^{RT} + r_i^{RB} + r_i^{LT})$$

where symbol $\times$ denotes the vector product in $\Re^2$. The unnormalized weight associated with the right-top corner is given by

$$\tilde{V}_i^{RT} = \frac{\pi}{2}\left|(\vec{\xi}_i^{RB} - \vec{\xi}_i^{RT}) \times (\vec{\xi}_i^{LT} - \vec{\xi}_i^{RT})\right| r_i^{RT}.$$

It has been shown in [11] that these weights preserve polar symmetry in the discrete solution on general conforming quadrilateral meshes. Unfortunately, the polar symmetry is not preserved on non-conformal meshes. Since the unnormalized weights do not necessary sum to the total cell area, we normalize them. For instance,

$$V_i^{RT} = V_i \frac{\tilde{V}_i^{RT}}{\tilde{V}_i^{RT} + \tilde{V}_i^{LT} + \tilde{V}_i^{LB} + \tilde{V}_i^{RB}}.$$

3 Solver

In this section we shall show that the system (2.9) – (2.13) can be easily reduced to a system of linear algebraic equations for interface intensities with a symmetric positive definite matrix.

The continuity conditions for intensities allow us to introduce a single intensity for each interface $\partial e_i \cap \partial e_j$, $i < j$. Let A_{ij} be the length of this interface and ϕ_{ij} denote the corresponding intensity. In a similar way, we may denote the flux from i-th cell to j-th cell as f_{ij}. For instance, in example shown in Fig. 3, we have $f_i^R = f_{ij} = f_{ik}$ and $f_j^L = f_{ji}$. The new notations allow us to rewrite the flux continuity conditions as

$$A_{ij} f_{ij} = -A_{ij} f_{ji}, \qquad i < j. \tag{3.1}$$

Using the above notations, we may rewrite the system (2.9) – (2.13) in a symmetric form. Let $B_i = A_i \vec{e}$ in definition (2.8) of the discrete gradient operator, i.e. $B_i = (A_i^R, A_i^T, A_i^L, A_i^B)^t$. Then,

$$\begin{array}{lclcll} M_i \vec{f_i} & + & B_i \phi_i^C & - & \sum_j A_{ij}\phi_{ij} & = & 0, \\ B_i^t \vec{f_i} & & & & & = & Q_i, \\ -A_{ij} f_{ij} - A_{ij} f_{ji} & & & & & = & 0, \end{array} \tag{3.2}$$

where the sum is taken over all interface intensities associated with the i-th cell, $i, j = 1, \ldots, N$, and $i < j$.

The system (3.2) is a typical example of a saddle point problem. Since it is symmetric, it can be solved by the Lanzcos iterative method. However, a few simple algebraic transformations will reduce (3.2) to a problem with a symmetric positive definite matrix. Note that the primary variables $\vec{f_i}$ and ϕ_i^C, $i = 1, \ldots, N$, are explicitly connected within a single cell. Therefore, they may be easily excluded from the system with $O(N)$ arithmetical operations resulting in

$$S\vec{\phi} = \vec{b} \tag{3.3}$$

where $\vec{\phi}$ denotes the global vector of interface intensities ϕ_{ij}, and $\vec{b}$ is the source vector. In addition to the properties mentioned above, the matrix S is sparse. A few examples of its stencils are shown in Fig. 4.

Lemma 3.1 *3.1 The matrix S is symmetric and positive definite.*

The proof of the lemma can be found in the Appendix.

The problem (3.3) can be solved by the conjugate gradient method. In the numerical experiments we use an algebraic multigrid preconditioner [16] to accelerate convergence rate of the iterative method.

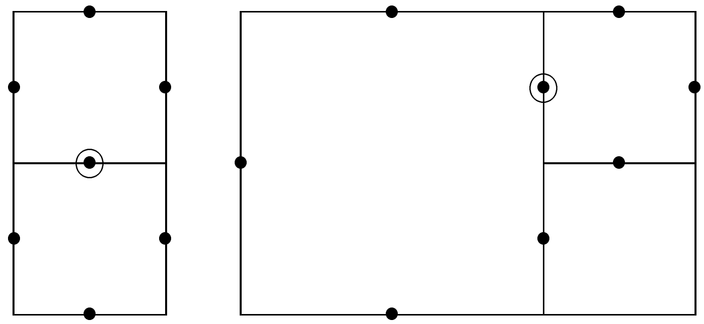

Figure 4: Stencils of matrix S.

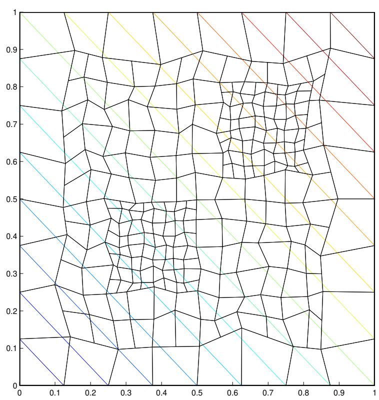

Figure 5: The isolines of a linear function.

In closing this section, we note that, if the mesh is orthogonal, all of the face-center intensities can be locally eliminated leaving an algebraic system for cell-center intensities [6, 12].

4 Computational results

In this section we present computational results which demonstrate the accuracy of our method and the efficiency of our solution techniques. The convergence of the SO method is briefly discussed in Section 5. The algebraic multigrid by Stüben and Ruge [16] was chosen as an example of a method applicable to arbitrary matrix stencils. However its theoretical justification is limited to M-matrices. In the case of highly disturbed meshes and random isotropic diffusion tensors, it should be replaced by more robust multigrid methods (see, e.g. [9]).

The first set of experiments verifies that our method is exact for linear functions. We consider the diffusion problem (1.1) in the unit square $(0,\, 1)^2$ subject to the Dirichlet boundary conditions. Let $D = 1$ and $\phi(x,\, y) = x + y$ be the exact solution. As shown in Fig. 5, the isolines of the computed solution are straight lines even on a randomly distorted grid. This confirms the theoretical results proved in [11].

The second set of calculations addresses the accuracy of the method on highly distorted adaptive meshes in the Cartesian coordinate system. We again consider

Table 1: Convergence on a sequence of adaptive and uniform grids.

l	AMR grids			Uniform grids		
	N	ϵ_ϕ	ϵ_f	N	ϵ_ϕ	ϵ_f
0	256	7.00e-2	8.18e-2	256	7.00e-2	8.18e-2
1	556	1.64e-2	3.42e-2	1024	1.79e-2	3.40e-2
2	988	3.74e-3	1.74e-2	4096	3.91e-3	1.62e-2
3	3952	9.96e-4	7.57e-3	16384	9.44e-4	7.30e-3
4	15808	2.40e-4	3.79e-3	65536	2.32e-4	3.76e-3

the diffusion problem (1.1) on the unit square subject to the Dirichlet boundary conditions. Let $D = 1$, then

$$\phi(x,\, y) = 1 - \tanh\left(\frac{(x-0.5)^2 + (y-0.5)^2}{0.01}\right)$$

is the exact solution. The function has a sharp peak in the middle of the domain and close to zero near the domain boundary. Calculations were performed on a sequence of randomly distorted locally refined and uniformly refined grids. Both sequences of grids are built in two steps. First, we refine grids in topological spaces. After that, we randomly distort positions on mesh points.

Both sequences begin with a 16×16 grid. We use a simple geometric approach to create a few first locally refined meshes. In a topological space, each mesh cell of the initial grid is uniquely identified by two indices i_0 and j_0, $1 \le i_0, j_0 \le 16$. On the first refinement level ($l = 1$), we split mesh cells with indices $4 \le i_0, j_0 \le 13$ into four cells. The new mesh cells are uniquely identified by two indices i_1 and j_1, $1 \le i_1, j_1 \le 20$. On the second refinement level, we split mesh cells with indices $5 \le i_1, j_1 \le 16$ into four cells. On the subsequent levels ($l > 2$) we uniformly refine all mesh cells.

The random grid is generated by moving each mesh point to a random position inside a square centered at the point. The sides of the square are aligned with the coordinate axis and equal 80% of the size of the smallest cell sharing the point. Note that the hanging mesh points are always located in the middle of the associated edges.

The relative L_2 errors ϵ_ϕ and ϵ_f for cell-centered intensities and edge-based fluxes, respectively, are given in Table 1. We observe the second order convergence rate for intensities and the first order convergence rate for fluxes. Even with our naive geometric refinement strategy, we achieve the same accuracy of the solutions on AMR and uniform grids but with 4 times less mesh elements. The better performance of our method can be obtained with a refinement strategy based on *a posteriori* error estimators (see, e.g. [17]). However, these error estimators are beyond the scope of this paper. The AMR and uniform grids at $l = 2$ are shown in Fig. 5 together with isolines of the discrete solutions.

The third set of calculations addresses the accuracy of the method on polar meshes in $r - z$ coordinate system. We consider a two dimensional problem in the $r - z$ coordinate system which is equivalent to the following one dimensional problem:

$$\frac{1}{R^2}\frac{\partial}{\partial R}\left(R^2 D \frac{\partial \phi}{\partial R}\right) = a + bR^2$$

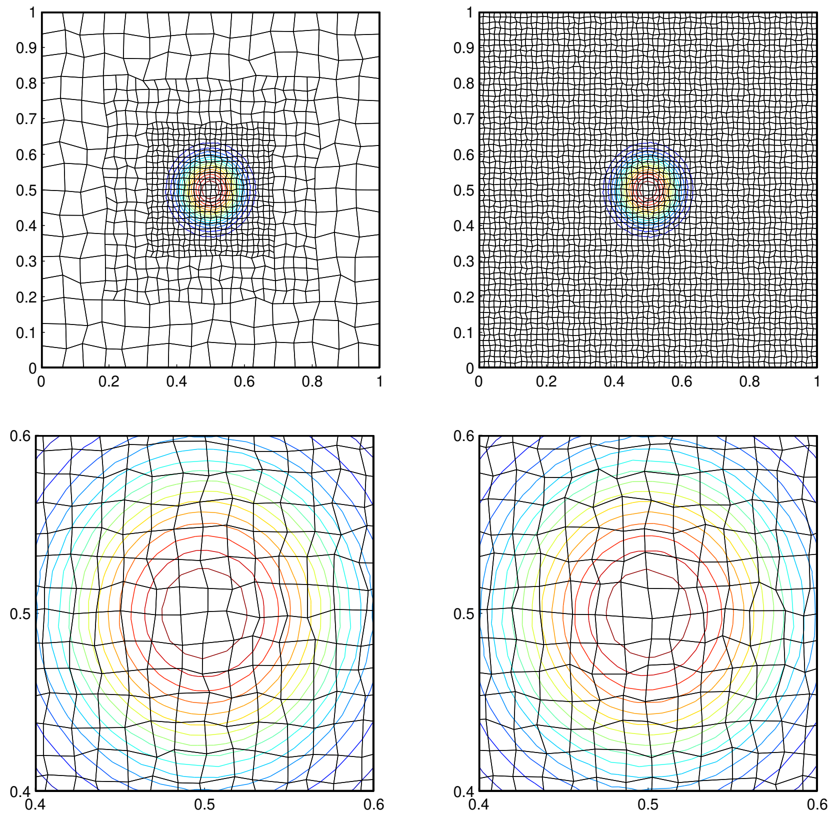

Figure 6: The grids and isolines of the solution ϕ for $l = 2$.

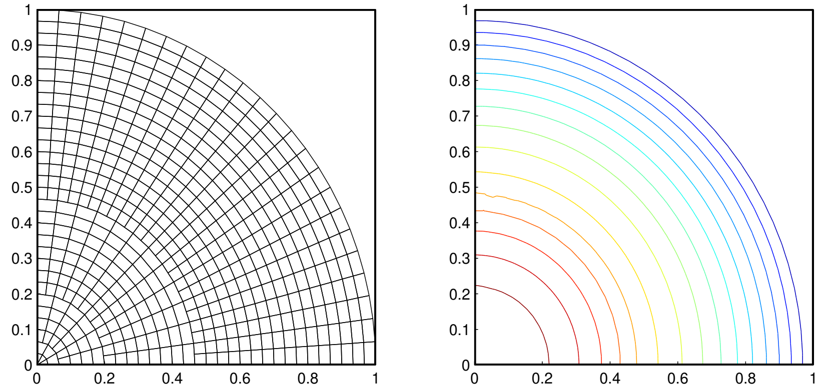

Figure 7: The polar grid and isolines: $a = b = 1$, $D_1 = 1$, and $D_2 = 2$.

where R denotes the spherical radius, $R = \sqrt{r^2 + z^2}$, and $0 \le R \le 1$. Let the diffusion coefficient equal to D_1 in the region defined by $0 < R < 0.5$ and equal to D_2 in the rest of the domain. In the $r - z$ coordinate system, we impose the Neumann boundary conditions along $z = 0$ and $r = 0$, and the Dirichlet boundary condition along $R = 1$. This problem admits an analytic solution:

$$\phi = \begin{cases} \dfrac{a}{3} + \dfrac{a}{24D_1} + \dfrac{a}{8D_2} + \dfrac{2b}{5} + \dfrac{b}{320D_1} + \dfrac{3b}{64D_2} - \dfrac{aR^2}{6D_1} - \dfrac{bR^4}{20D_1}, & 0 < R < 0.5, \\ \dfrac{a}{3} + \dfrac{a}{6D_2} + \dfrac{2b}{5} + \dfrac{b}{20D_2} - \dfrac{aR^2}{6D_2} - \dfrac{bR^4}{20D_2}, & 0.5 < R < 1. \end{cases}$$

The computed solution shown in Fig. 7 gives a good approximation to the exact solution. However, the detailed analysis shows that the discrete solution exhibits symmetry breaking. In order to study this effect, we plot the trace of the solution at $R = 0.5$ as the function of the polar angle. The trace is the piecewise constant function shown on the left picture in Fig. 8. The straight line is the trace of a discrete solution on the uniform grid having the same number of mesh steps in the r-direction. The number of mesh steps in the angular direction is the same as that on locally refined grid at $R = 1$.

Note that the amplitude of oscillations is decreased by the grid refinement (see right picture in Fig. 8). The two oscillating functions in this picture are traces of the discrete solutions on level $l = 3$ and $l = 4$. The straight line is the trace of the exact solution at $R = 0.5$.

The forth set of calculations addresses the application of quadrilateral interface-fitted meshes to problems with strong material discontinuities. We consider the Poisson equation (1.1) in the unit square. Let the diffusion coefficient equal to D_1 inside the disk of radius 0.25 centered at point (0.5, 0.5) and let it equal D_2 in the rest of the domain. Let $r = \sqrt{(x-0.5)^2 + (y-0.5)^2}$ and $Q = r^2$. We choose the Dirichlet boundary conditions in such a way that the exact solution is a function of r. The computational mesh and the discrete solution for $D_1 = 1$ and $D_2 = 100$ are shown in Fig. 9. The solution changes sign in the vicinity of the material discontinuity. Therefore the optimal computational strategy requires the mesh refinement as well as a mesh adaptation to the line of material discontinuity.

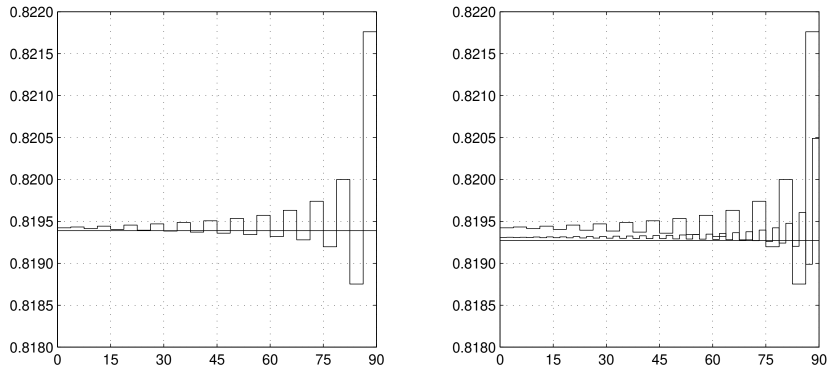

Figure 8: The symmetry breaking: solution traces at $R = 0.5$.

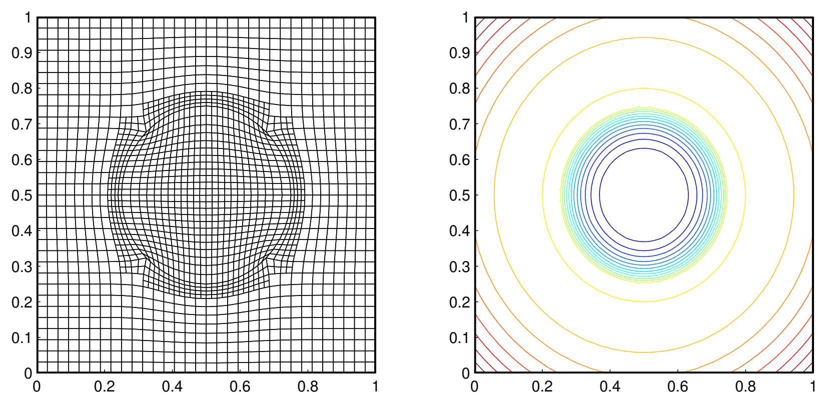

Figure 9: The AMR grid and isolines of the solution ϕ for the problem with strong material discontinuity.

Table 2: Iterative convergence details.

l	Adaptive grids			Uniform grids		
	N	#itr	CPU	N	#itr	CPU
1	256	12	0.05s	256	12	0.05s
2	556	15	0.14s	1024	13	0.27s
3	988	16	0.28s	4096	14	1.25s
4	3952	16	1.33s	16384	15	5.58s
5	15808	17	6.21s	65536	17	25.3s

The fifth set of calculations is primary intended to study the performance of the V-cycle of the algebraic multigrid method by Stüben and Ruge. The results from the second set of calculations are presented in Table 2. The stopping criterion for the preconditioned conjugate gradient method was the relative decrease in the norm of the residual by factor 10^{-12}. The number of iterations, #itr, grows much slower than the number of mesh cells, N. The computational time, denoted by CPU, includes the arithmetical costs for generation of the matrix S, solving the problem (3.3) and recovering the discrete flux and cell-centered intensities. The arithmetical costs per iteration grows linear in N except on coarse grids where cache memory effects play the important role.

5 Conclusions and Future Work

Our SO method has been shown to be second-order accurate on non-smooth quadrilateral meshes with hanging nodes in both Cartesian and R-Z geometries. Although the scheme has both cell-center and face-center intensity unknowns, the cell-center unknowns are locally eliminated, resulting in a reduced system consisting only of the face-center unknowns. This reduced system has a symmetric positive-definite coefficient matrix. It has also been shown that the algebraic multigrid method of Stüben and Ruge is quite effective for this system with the time-to-solution scaling linearly with the number of unknowns. Thus our SO scheme represents a viable basis for the development of adaptive diffusion solution algorithms for general non-orthogonal quadrilateral meshes.

On R-Z meshes, our hanging-node scheme does not preserve spherical symmetry. The preservation of such symmetry is a topic for future research. Another topic for future research is the generalization of the hexahedral-mesh SO scheme [10] to hanging-node meshes.

In the case of conformal meshes, the theoretical analysis of the convergence of the SO discretizations has been done in [3]. The main idea was to establish a connection between the SO method and the lower order mixed finite element (MFE) method. Both methods use the same definitions for cell centered intensities and interface fluxes. The difference lies in the definition of scalar products in the space of fluxes. Each of them can be considered as a quadrature rule. Then, the convergence estimates for the SO method follow from the theory of FE approximations. It is pertinent to note here that this connection exists only for triangular and quadrilateral meshes where the corresponding FE spaces are known. However, the SO discretizatons have demonstrated efficiency and robustness for many other types of meshes.

For the case of AMR meshes, it is again possible to establish a connection with a lower order MFE method, e.g., the method from [2]. The interface intensities in the SO method are degrees of freedom of a mortar FE space. It implies that the MFE method results in system (3.2) with some matrices $\tilde{M}_i$ instead of M_i. These matrices describe a scalar product in the space of Raviart-Thomas finite elements. The optimal convergence estimates for the SO method follow from error estimates for the MFR method [2] and accuracy estimates for the quadrature rule (2.5) derived in [3]. We shall address this issue in more detail in the future work.

Acknowledgments

The authors thank Dr. Shengtai Li for his assistance in generating locally fitted meshes.

References

[1] R. W. Anderson, R. B. Pember, and N. S. Elliott. An arbitrary Lagrangian-Eulerian method with local structured adaptive mesh refinement for modeling shock hydrodynamics. Presented at the 40'th AIAA Aerospace Sciences Meeting and Exhibit, January 14-17, 2002, Reno Nevada. AIAA paper 2002-0738, published by the American Institute of Aeronautics and Astronautics,1801 Alexander Bell Drive, Suite 500, Reston, VA 20191-4344.

[2] T. Arbogast, L. Cowsar, M. Wheeler, and I. Yotov. Mixed finite element methods on non-matching multiblock grids. *SIAM J. Numer. Anal.*, 37:1295–1315, 2000.

[3] M. Berndt, K. Lipnikov, D. Moulton, and M. Shashkov. Convergence of mimetic finite difference discretizations of the diffusion equation. *J. Numer. Math.*, 9:253–284, 2001.

[4] D. Braess. *Finite Elements : Theory, Fast Solvers, and Applications in Solid Mechanics*. Cambridge University Press, Cambridge, U.K. ; New York, 1997.

[5] H.-W. Choi and M. Paraschivoiu. A posteriori finite element output bounds with adaprive mesh refinement: application to a heat transfer problem in a three-dimensional rectangular duct. *Comput. Methods Appl. Mech. Engrg.*, 191:4905–4925, 2002.

[6] M. Edwards. Elimination of adaptive grid interface errors in the discrete cell centered pressure equation. *J. Comput. Phys.*, 126:356–372, 1996.

[7] R. E. Ewing, R. D. Lazarov, and P. S. Vassilevski. Local refinement techniques for elliptic problems on cell-centered grids I, error analysis. *Mathematics of Computation*, 56:437–461, 1991.

[8] J. Hyman, M. Shashkov, and S. Steinberg. The numerical solution of diffusion problems in strongly heterogeneous non-isotropic materials. *J. Comput. Phys.*, 132:130–148, 1997.

[9] Y. Kuznetsov. Two-level preconditioners with projectors for unstructured grids. *Russian J. Numer. Anal. Math. Modelling*, 15(3–4):247–256, 2000.

[10] J. Morel, M. Hall, and M. Shashkov. A local support-operators diffusion disretization scheme for hexahedral meshes. *J. Comput. Phys.*, 170:338–372, 2001.

[11] J. Morel, R. Roberts, and M. Shashkov. A local support-operators diffusion disretization scheme for quadrilateral $r-z$ meshes. *J. Comput. Phys.*, 144:17–51, 1998.

[12] G. Olson and J. Morel. Solution of the radiation equation on an amr eulerian mesh with material interfaces. Technical report, Los Alamos National Laboratory, 1999.

[13] R. B. Pember and J. B. Bell. An adaptive Cartesian grid method for unsteady compressible flow in irregular regions. *J. Comput. Phys.*, 120:278–304, 1995.

[14] J. J. Quirk. A parallel adaptive grid algorithm for computational shock hydrodynamics. *Appl. Numer. Math.*, 20:427–453, 1993.

[15] M. Shashkov and S. Steinberg. Solving diffusion equations with rough coefficients in rough grids. *J. Comput. Phys.*, 129:383–405, 1996.

[16] K. Stüben. Algebraic multigrid (AMG): experiences and comparisons. *Appl. Math. Comput.*, 13:419–452, 1983.

[17] R. Verfurth. A posteriori error estimation and adaptive mesh-refinement techniques. *J. Comput. Appl. Math.*, 50:67–83, 1994.

[18] D. D. Zeeuw and K. G. Powell. An adaptively refined Cartesian mesh solver for the Euler Equations. *J. Comput. Phys.*, 104:56–68, 1993.

Appendix

<u>Proof of Lemma 3.1</u>. The system (3.2) can be rewritten in a matrix form

$$\begin{pmatrix} M & B & C \\ B^t & 0 & 0 \\ C^t & 0 & 0 \end{pmatrix} \begin{pmatrix} \vec{f} \\ \vec{\phi}^C \\ \vec{\phi} \end{pmatrix} = \begin{pmatrix} 0 \\ \vec{Q} \\ 0 \end{pmatrix}$$

where $\vec{f}$ and $\vec{\phi}$ are the global vectors of interface fluxes and intensities, respectively, and $\vec{\phi}^C$ is the global vector of cell-centered intensities. We assume that the solution components are ordered in such a way that the matrix M has the block diagonal structure with 4×4 diagonal blocks M_i, $i = 1, \ldots, N$. then, the matrix S from (3.3) can be expressed via matrices M, B and C, i.e.

$$S = C^t \ (M^{-1} - M^{-1}B(B^tM^{-1}B)^{-1}B^tM^{-1}) \ C.$$

First, we shall show that the matrix S is positive semi-definite, i.e.

$$< S\vec{\phi}, \vec{\phi} > \ \geq \ 0, \qquad \forall \vec{\phi} \in \Re^{N_\phi}.$$

where N_ϕ is the total number of interface intensities. Note, that the matrix C, $C \in \Re^{N_\psi \times N_\phi}$, and has almost twice more rows than columns. Therefore,

$$\min_{\vec{\phi} \in \Re^{N_\phi}} < S\vec{\phi}, \vec{\phi} > \ \ \geq \ \min_{\vec{\psi} \in \Re^{N_\psi}} < (M^{-1} - B(B^tM^{-1}B)^{-1}B^tM^{-1})\vec{\psi}, \vec{\psi} > .$$

We observe that $B^t M^{-1} B$ is a diagonal matrix. Therefore,

$$M_1 = M^{-1} B (B^t M^{-1} B)^{-1} B^t M^{-1}$$

is the block diagonal matrix with 4×4 blocks, i.e., it has the same structure as M^{-1}. It is easy to show that all diagonal blocks of $M - M_1$ are symmetric positive semi-definite matrices. Moreover, the null space of the i-th diagonal block is represented by the vector B_i from (3.2). Therefore, $S \geq 0$.

Second, we shall show that there exist only one $\vec{\phi} \in \Re^{N_\phi}$ such that $C\vec{\phi} \in \ker(M - M_1)$. Analysis of the structure of matrices B and C shows that the interface intensities associated with a mesh element are equal to each other. This is possible if and only if $\vec{\phi} = c(1, \ldots, 1)$ where c is a constant. The homogeneous Dirichlet boundary conditions imply that $c = 0$. This proves the assertion of the lemma.